Submitted: 06/24/2024
Accepted: 03/06/2025
Published: 03/31/2025

Research Article

[1]Genomic Instability in Development and Disease, European Institute for the Biology of Aging, University of Groningen, Groningen, Netherlands

Keywords

Lymphoma, Chromosomal instability, IL-6 signaling, Inflammatory response, cGas/STING

Email Correspondence

v.muller.5@student.rug.nl

https://doi.org/10.26443/msurj.v20i1.246

Veronika Müller[1]

Chromosomal Instability and IL6-Mediated Inflammatory Signaling in Human Lymphoma Cells

Abstract

Chromosomal Instability (CIN) is a hallmark of cancer that significantly impacts tumor evolution and prognosis in lymphomas. This study investigates the relationship between CIN and inflammatory signaling, particularly the IL6 pathway, in human lymphoma cell lines. Genomic analysis revealed diverse mutational landscapes across cell lines, reflecting varying degrees of genomic instability. qPCR analysis demonstrated consistent upregulation of IL6 expression upon Vincristine treatment across all tested cell lines. IncuCyte analysis of cell viability after treatment with the CIN-inducing agent BAY1217389 revealed dose-dependent effects, with certain levels of CIN potentially enhancing cell growth. These findings suggest that CIN activates IL6-mediated inflammatory signaling in lymphoma cells, contributing to a pro-tumor microenvironment and potentially modulating therapeutic outcomes.

Introduction

Lymphomas are a heterogeneous group of malignancies characterized by the clonal expansion of lymphocytes and marked genomic disruption. Chromosomal Instability (CIN), a hallmark of cancer, is particularly prevalent in lymphomas due to the physiological DNA breaks and translocations that occur in lymphocytes. These physiological processes encompass V(D)J (variable–diversity–joining) recombination[1], class switch recombination, and somatic hypermutation. While these rearrangements are tightly regulated under normal conditions, they can result in errors, leading CIN[1]. The stability of chromosomes is ensured by the physiological activity of genome maintenance pathways, like cell cycle checkpoints, DNA repair mechanisms, and the coordinated activity of the cell division machinery. These areas of DNA processing, including recombination, repair, and replication can be vulnerable to deficiencies in chromosomal stability. As a result, defects in these pathways can cause CIN[2].

CIN substantially impacts tumor evolution by dysregulating the immune response and promoting cell-intrinsic inflammatory signaling. The origins of cells with CIN-phenotype and micronuclei stem from various mitotic errors[2]. During anaphase, under-replicated DNA from S phase can form ultra-fine bridges, which may break in subsequent cell cycles, resulting in micronuclei. Unrepaired double-strand breaks can lead to chromosome breakage during mitosis, potentially causing radial chromosomes with multiple centromeres. These structures can form bulky chromosomal bridges that produce micronuclei. Additionally, fully duplicated chromosomes may occasionally lag at the metaphase plate due to kinetochore-microtubule attachment issues, leading to whole chromosome micronuclei in the next cell cycle (Figure 1)[2].

The rupture of micronuclei occurs due to nuclear envelope (NE) instability[3]. Chromosomes distant from spindle microtubules recruit non-core NE proteins like nuclear pore complex, Lamin B, and Lamin B receptor, disrupting the density of these proteins and leading to NE fragility. Aurora B kinase, which senses lagging chromosomes, establishes a CDK1 phosphorylation gradient by stabilizing Cyclin B[4]. This disrupts the phosphorylation of proteins involved in nuclear envelope assembly and disassembly, further destabilizing the NE[4]. Consequently, the fragile micronuclei are prone to rupture, releasing their double-stranded DNA content into the cytoplasm and, activating the cGAS/STING-pathway (Figure 2)[5].

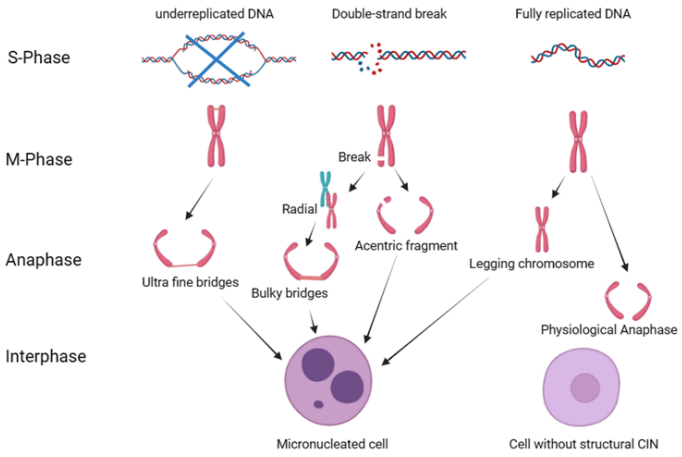

Figure 1. Schematic representation of the origins of cells with CIN-phenotype and micronuclei.

In physiological conditions, the cGAS-STING pathway detects cytoplasmic DNA. When cytoplasmic DNA binds to cGAS, it catalyzes the synthesis of cGAMP from ATP and GTP. This cGAMP acts as a second messenger, binding to STING on the ER membrane and triggering its activation. Activated STING then translocates from the ER to the Golgi apparatus, recruiting and activating TBK1 and IKK kinases. These kinases subsequently activate the IRF3 and NF-κB signaling cascades, leading to the expression of type I interferons and inflammatory cytokines that enhance immune responses[5]. However, under chronic CIN conditions, this pathway becomes

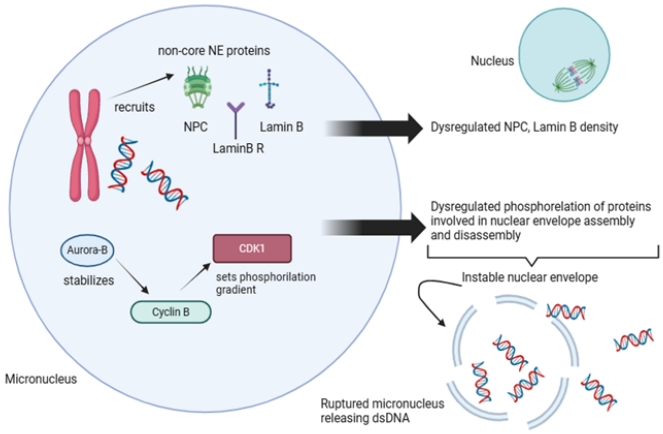

Figure 2. Schematic representation of the pathways involved in the rupture of a micronucleus as a result of an insatiable nuclear envelope (NE).

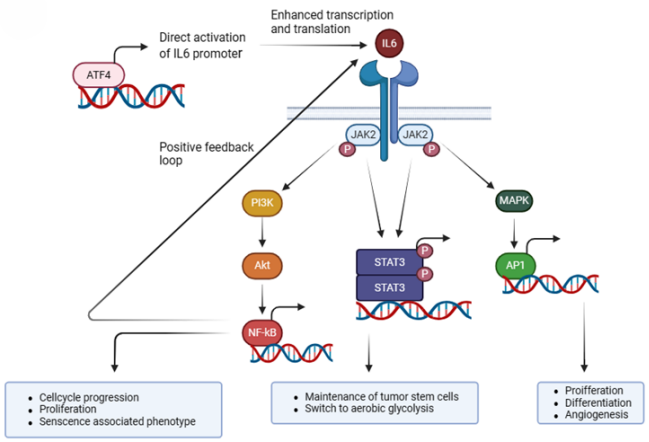

Figure 4. IL6, NF-κB and STAT3 in CIN associated tumorigenesis.

dysregulated, as illustrated in Figure 3.

The cGAS/STING pathway under chronic CIN leads to immunosuppression, a pro-tumor microenvironment, and metastasis[5]. Cytoplasmic DNA, released from ruptured micronuclei, is detected by cGAS, which catalyzes cGAMP formation and activates STING[5]. Chronic activation of this pathway results in persistent genomic instability and cellular stress, potentially overwhelming cellular machinery and leading to ER stress and unfolded protein response (UPR) activation[6]. Cancer cells exploit the UPR to adapt to the hostile tumor microenvironment, promoting cell survival and therapy resistance[7]. Prolonged activation of STING signaling may trigger negative feedback mechanisms, including epigenetic modifications that downregulate STING expression[8], ultimately resulting in immunosuppression and a pro-tumor microenvironment (Figure 3).

IL6, NF-κB, and STAT3 play crucial roles in CIN-associated tumorigenesis. ATF4, downstream of PERK, directly activates the IL6 promoter[9]. IL6 signaling promotes tumor growth, metastasis, and therapy resistance by activating multiple pathways. The PI3K/AKT pathway, activated by IL6, promotes cell survival and growth[10]. AKT activation leads to NF-κB activation, which regulates genes associated with inflammation, cell survival, and proliferation[11]. IL6 also activates the JAK/STAT pathway, leading to STAT3 phosphorylation. Activated STAT3 maintains the stemness

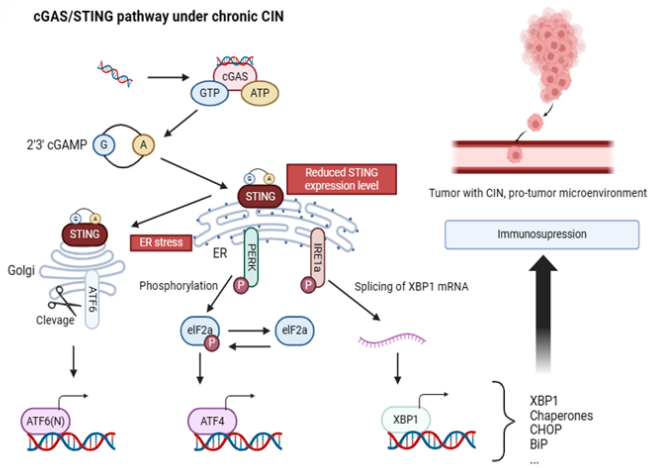

Figure 3. Schematic representation of the cGAS/STING pathway under chronic CIN, leading to immunosuppression, pro-tumor microenvironment, and metastasis.

of tumor-initiating cells and promotes metabolic reprogramming in cancer cells[12]. Additionally, IL6 activates the MAPK pathway, leading to AP-1 activation, which promotes cell proliferation, differentiation, and angiogenesis[13]. These interconnected pathways collectively contribute to tumor growth and metastasis in the context of CIN (Figure 4).

A recent study by Hong et al. highlighted the role of CIN in driving inflammatory signaling pathways, particularly the IL6/STAT3 axis, in breast cancer and a Lymphoma mouse model[5]. However, the specific implications of this pathway in human lymphoma cells remain unclear. This gap in knowledge represents a critical area for investigation, given the established link between CIN and prognosis/treatment response in lymphomas.

This study aims to investigate whether CIN in human lymphoma cells activates the IL6-mediated inflammatory signaling pathway and influences cell viability, potentially contributing to a pro-tumor microenvironment that modulates therapeutic outcomes. To address this question, a multi-faceted approach was employed combining genomics analysis, quantitative assessment of inflammatory cytokine expression, and evaluation of cell viability under CIN-inducing conditions.

This research utilizes multiple lymphoma cell lines, inducing CIN through inhibition of Monopolar spindle 1 (MPS1) kinase. The proliferative response to CIN induction and levels of key cytokines, including IL6 and its receptor was analyzed, using qPCR. Additionally, the response of these cells to Vincristine, a common chemotherapeutic agent, was assessed to infer possible implications for therapy modulation[5].

Understanding the relationship between CIN and inflammatory signaling in lymphoma is crucial for developing more effective treatment strategies. By elucidating these mechanisms, we may identify novel therapeutic targets and improve patient outcomes.

Methods

Genomics Analysis of Publicly Available Datasets

To investigate the molecular and genetic landscape in human lymphoma cell lines and set a foundation for cell line comparison, a genomics analysis of publicly available datasets was performed. Genomic data for the lymphoma cell lines Daudi, Ramos, SU-DHL-10, SUDHL-6, OCI-LY3 was downloaded from the cBioportal for Cancer genomics. To analyze datasets, we examined the data for mutation count and fraction of the genome altered, as well as specific oncogenes and genes significantly altered in the

lymphoma cell lines.

Cell Culture

The cell lines used were selected based on their relevance to the biological context under investigation. The inclusion of multiple cell lines enables a comparative analysis, ensuring that observed effects are not cell-type specific but rather reflect broader principles. These models were chosen based on their established use in previous studies.

The human lymphoma cell lines Ramos (Human Burkitt lymphoma cell line, hypodiploid karyotype, 45 Chromosomes), Daudi (Human Burkitt lymphoma cell line, nearly diploid karyotype with 66% stability of the cells within their stem line, 20% polyploid), SU-DHL-6 (B-cell non-Hodgkin lymphoma cell line, hyperdiploid, 47 Chromosomes), SU-DHL-10 (Human B-cell lymphoma, hyperdiploid karyotype), and OCI-LY3 (Human B cell lymphoma, hypertriploid karyotype) were cultured using RPMI medium with 20% fetal bovine serum, 1% penicillin streptomycin at 37 °C with 5% CO_2 for 72 hours in a humidified incubator.

qPCR

To assess the baseline and treatment induced inflammatory response, as well as the dose-dependent drug response, the human lymphoma cell lines Ramos, Daudi, SU-DHL-6, SU-DHL-10, and OCI-LY3 were tagged with mRaspberry and subsequently treated with 0nM, 2nM and 5nM of Vincristine. The dosage was established in the previous study by Hong et al., treating cancer cells with CIN[5]. A qPCR for the detection of cytokines and the IL6 receptor was performed with IL6, CCL5, CXCL10, IL-8 and IL6R primers. We used Tubulin and HPRT1 as housekeeping genes and the reaction master mix iTaq Universal SYBR Green Supermix (Bio Rad, California) for detection. Total RNAs were extracted from all cell lines using the NucleoSpin RNA Plus RNA Isolation kit (Macherey-Nagel™, UK), and total cDNAs were synthesized using the LunaScript RT Master Mix Kit (Bioke, Netherlands) in accordance with the respective manufacturer's protocol. IL6, CCL5, CXCL10, IL-8, and IL6R transcripts as well as the housekeeping genes, Tubulin and HPRT1, were detected by dye based quantitative real-time polymerase chain reaction.

Transduction for IncuCyte Analysis

To ensure that the IncuCyte analysis is performed on a homogenous population of cells expressing the desired genetic modifications at consistent levels, a transduction was performed. We transduced target Eph4 cells with lentiviral vectors encoding the genes of interest (dnMCAK, MPS1-D637A-T649A) or empty vector controls under different promoters (pGK, pUBC, pEF1a). We transfected HEK293T cells with the lentiviral transfer plasmid along with packaging plasmids psPAX2 and pMD2.G using TurboFect transfection reagent. Viral supernatants were harvested 48- and 72-hours post-transfection, filtered through a 0.45 µm filter, and supplemented with 8 µg/ml polybrene, before transducing Eph4 cells in two rounds. Two days after the second round of transduction, we selected transduced cells by replacing the medium with fresh medium containing 0.75−1.5 µg/ml puromycin until all non-transduced control cells had died. Stably transduced cell populations were then expanded under normal culture conditions without antibiotic selection. Thereafter, cells were transfected with H2B-mCherry fluorescent protein to enable cell imaging and analysis.

IncuCyte Analysis

The IncuCyte Live-Cell Analysis System was chosen for assessing cell viability and proliferation as it provides real-time, non-invasive monitoring of cell growth, allowing for the capture of temporal dynamics in response to treatment.

For the evaluation of the dose-dependent effects of BAY1217389-induced CIN on cell growth and viability in different human lymphoma cell lines, we treated Daudi, Ramos, and SU-DHL-10 with varying concentrations of the CIN-inducing Monopolar spindle 1 (MPS1) kinase inhibitor BAY1217389 (Selleckchem): 0 nM (control), 1 nM, 2.5 nM, 5 nM, 10 nM, 15 nM, 20 nM, and 25 nM. The concentrations of BAY1217389 (0-25 nM) were selected based on previously reported IC50 values in various cancer cell lines (ranging from 3.7 to 12 nM) and prior literature[1,5]. The cells were seeded in triplicate at four different initial densities: 8,000, 14,000, 20,000, and 26,000 cells per well (c/w) in a 96-well plate. The 96-well plate was placed in the IncuCyte Live-Cell Analysis System (Sartorius) and monitored for 72 hours. Phase-contrast and fluorescent images were acquired every 3 hours to track cell growth and viability. The IncuCyte software quantified the fluorescent object count, which corresponds to the number of viable cells, at each time point. We curated the obtained data and double-normalized the raw fluorescent object count data to account for potential variations in initial seeding densities and to facilitate comparison across different conditions and cell lines. The normalization process involved:

1. normalizing the raw data to the time 0 (initial seeding) count for each well;

2. normalizing the time 0-normalized data to the average of the respective vehicle control (0 nM BAY1217389) for each cell line and initial seeding density.

The normalization process allowed for comparison between vehicle control and treatment conditions as well as the observation of growth patterns. Subsequently, to gain insights into the temporal dynamics of the drug's effects and identify the time points at which the drug's anti-proliferative or cytotoxic activity is most pronounced, we performed a Pearson correlation analysis between the drug dose and the normalized cell count at each timepoint and for each seeding density. The Pearson correlation analysis provides a statistically robust method for quantifying the time-dependent relationship between BAY1217389 concentration and cell viability. This approach captures the dynamics of cellular responses to CIN induction. It reveals possible transition points where treatment effects become pronounced and identifies cell-line specific response patterns. Subsequently, a single factor ANOVA was applied to test statistical significance.

Results

Genomics Analysis of Publicly Available Datasets

Analysis of publicly available genomic datasets revealed diverse genomic landscapes across five human lymphoma cell lines: Ramos, Daudi, SU-DHL-6, SU-DHL-10, and OCI-LY3. These cell lines exhibited varying degrees of genetic alterations, providing insights into their potential biological behavior and therapeutic responses.

The selected lymphoma cell lines exhibit a range of karyotypic complexities, reflecting the genetic heterogeneity observed across lymphoma subtypes. Daudi and Ramos, for instance, share the hallmark t(8;14) IGH-MYC translocation characteristic of Burkitt lymphoma, while SU-DHL-6 and SU-DHL-10 harbor the t(14;18) IGH-BCL2 rearrangement, commonly associated with diffuse large B-cell lymphoma (DLBCL) and follicular lymphoma. OCI-LY3, with its hypertriploid karyotype (Table 1) and concurrent IGH-SPIB and BCL amplifications, represents a more genetically complex model.

OCI-LY3, derived from anaplastic large-cell lymphoma, demonstrated the

Table 1. Genetic Landscape of the investigated human lymphoma cell lines (Leibniz Institute DSMZ: Details, https://www.dsmz.de/)

Cell line	Cytogenetics
Daudi	human near diploid karyotype with 20% polyploidy - 46(45-48)<2n>XY/XXY, +7, -9, t(8;14)(q24;q32)
Ramos	45(44-46)<2n>X, -Y, del(2)(p16p23), t(8;14)(q24;q32.2), add(14)(p11), der(16)t(7;16)(q11.2;p13.2), der(17)t(13;17)(q33;p11.3)t(13;3)(q13;q?25), del(20)(q12); carries t(8;14) effecting IGH-MYC rearrangement
SU-DHL-6	human hyperdiploid karyotype with 2% polyploidy - 47(42-48)<2n>X, -Y, +6, +7, del(4)(q23), del(6)(p21.3p22.2), i(6p), del(7)(q?22q?32), der(8)t(8;9)(q24;p13), der(9)t(8;19;9)(q24;q13;p13), dup(11)(q24q25), t(14;18)(q32;q21), der(22)t(?7;22)(?q32;p11) - sideline with dic(8;9)(q24;p13), ider(8)(q10)t(8;9(q24;p13) - matches published karyotype - carries t(14;18) effecting IGH-BCL2 fusion
SU-DHL-10	human flat-modded hyperdiploid karyotype - 47(43-48)<2n>XY, +7,der(8)t(X;8)(q25;p23)t(8;X)(q24;q26)t(X;14)(q28;q32), del(10)(q22q24), der(11)t(Y;11)(q11;q25), der(14)t(8;14)(q24;q32), der(18)t(14;18)(q32;q21) — carries concurrent rearrangements of IGH with MYC and BCL2 — resembles published karyotype
OCI-LY3	human flat-moded hypertriploid karyotype; 72-77<3n>XXYY, +1, +9, -10, +13, +14, -17, +19, +20, +22, der(1)t(1;17)(p13;q12)x2, der(4)t(4;18)(q31;q21)x2, del(6)(q13)x2, der(6)t(6;6)(p24;q12), der(7)t(6;7)(p24;p22), der(14)t(14;19)(q32;q13.3)x2, del(18)(q21), der(19)t(4;19)(q21;q13)t(4;18) (q31;q21)x2, der(19)t(14;19), dup(20)(q11q13)x2; sdl with der(6)t(6;12)(p21;q21), der(7)t(5;7)(?p15;p24) etc; resembles published karyotypes; carries cryptic t(14;19) with rearrangement of IGH and SPIB, and t(4;18) with copy number amplification of the BCL2 region

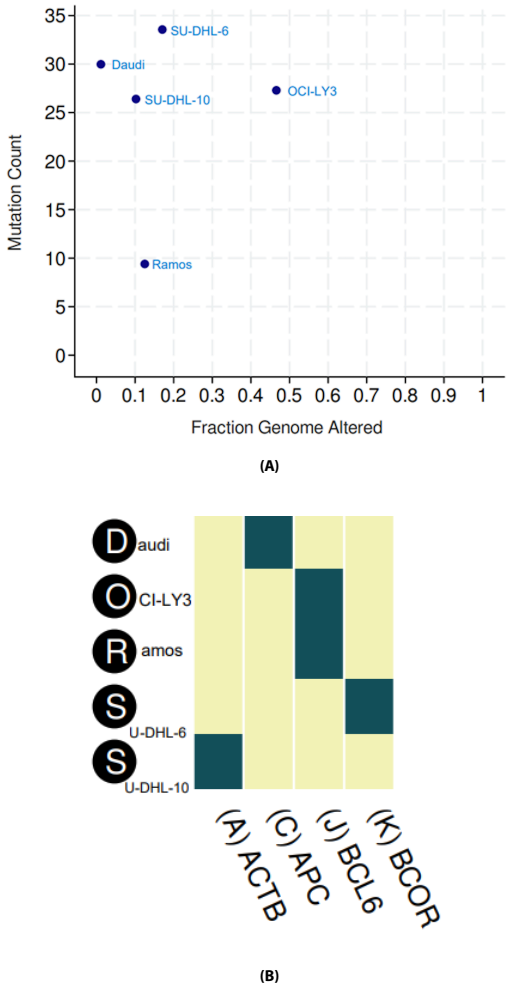

Figure 5. Genomic landscape of Ramos, Daudi, SU-DHL-6, SU-DHL-10, and OCI-LY3. (A) The mutation count is plotted versus fraction of genome altered. (B) Specific mutated genes in the respective cell lines.

most extensive history of genomic instability with a hypertriploid karyotype, complex chromosomal rearrangements, and the highest fraction of genome altered (0.461) (Figure 5A). It also carried a mutation in the BCL6 gene (Figure 5B).

SU-DHL-6, originating from B-cell non-Hodgkin lymphoma, showed a hyperdiploid karyotype with the t(14;18)(q32;q21) translocation, as depicted in Table 1, and a mutation in the BCOR gene (Figure 5A). It exhibited a high mutation count (34) and moderate fraction of genome altered (0.1679) (Figure 5B).

SU-DHL-10, another B-cell lymphoma line, displayed a hyperdiploid karyotype with rearrangements involving MYC, BCL2, and IGH loci, as well as a mutation in the ACTB gene (Figure 5A). It showed moderate levels of both mutation count (26) and fraction of genome altered (0.0970) (Figure 5B).

Daudi, characterized by a near-diploid karyotype with 20% polyploidy, carried the t(8;14)(q24;q32) (Table 1) translocation and a mutation in the APC gene. Despite a high mutation count (30), it had the lowest fraction of genome altered (0.0102) among the studied cell lines (Figure 5B).

Ramos, with a hypodiploid karyotype and the t(8;14)(q24;q32.2) translocation (Table 1), harbored an APC gene mutation (Figure 5A). It exhibited the lowest mutation count (9) but a moderate fraction of genome altered (0.1145) (Figure 5B).

This diversity in genomic profiles across the lymphoma cell lines suggests that different molecular pathways and mechanisms may contribute to the development and progression of these malignancies. These unique genetic makeups may also influence chromosomal instability-induced inflammatory signaling pathways and responses to therapeutic interventions.

qPCR

The qPCR analysis was performed on five human lymphoma cell lines (Ramos, Daudi, SU-DHL-10, and OCI-LY3) to assess their inflammatory response to Chromosomal Instability (CIN) induced by Vincristine treatment (0 nM, 2 nM, and 5 nM). The expression of IL6, CCL5, CXCL10, IL-8, and IL6R was evaluated.

IL6 expression was consistently upregulated across all viable cell lines following Vincristine treatment (Figure 6). SU-DHL-10 exhibited the highest fold-change in IL6 expression (12.16-fold at 2 nM Vincristine), followed by OCI-LY3 (3.78-fold at 2 nM), Daudi (2.39-fold at 5 nM and 1.58-fold at 2 nM), and Ramos (1.83-fold at 2 nM) (Figure 6).

The Daudi cell line demonstrated the most consistent dose-dependent in-

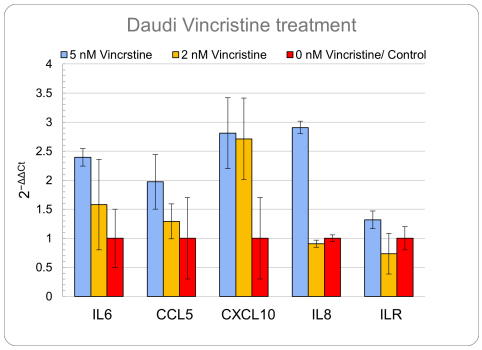

(A)

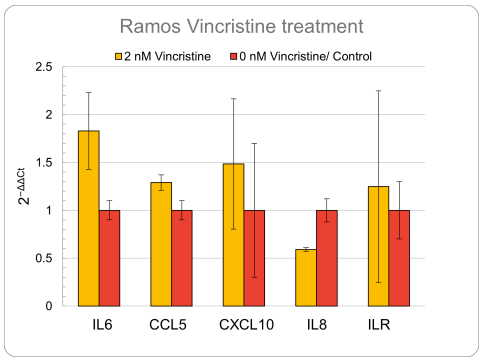

(B)

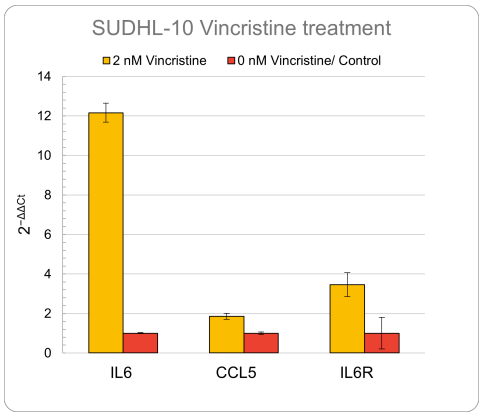

(C)

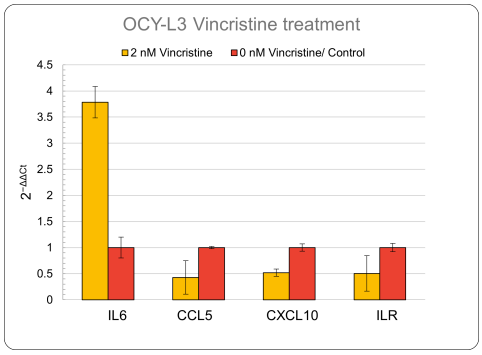

(D)

Figure 6. The Expression Fold Change of IL6, CCL5, CXCL10, IL8 and IL6-R. The double delta CT analysis of the qPCR results for cytokine expression of IL6, CCL5, CXCL10, IL8 and IL6-R and the technical standard deviation for each condition after treatment with 2 nM and 5 nM Vincristine, compared to the untreated control (0 nM) of the cell lines Daudi, Ramos, SU-DHL-10, and OCI-LY3. The data is presented as the mean fold change, also displaying the technical standard deviation as error bars. (A) Expression fold change of cytokines and IL6-R in Daudi. (B) Expression fold change of cytokines and IL6-R in Ramos. (C) Expression fold change of cytokines and IL6-R in SU-DHL-10. (D) Expression fold change of cytokines and IL6R in OCI-LY3.

crease in cytokine expression. At 5 nM Vincristine, IL6, CCL5, CXCL10, and IL-8 expression increased by 139%, 97%, 181%, and 191%, respectively, compared to the control. IL6R expression also increased by 32% (Figure 6A).

CCL5 expression varied across cell lines, showing dose-dependent increases in Daudi and moderate increases in Ramos and SU-DHL-10, but decreased in OCI-LY3. CXCL10 expression increased dose-dependently in Daudi, moderately in Ramos, but decreased in OCI-LY3 (Figure 6). IL-8 expression increased dose-dependently in Daudi but decreased in Ramos. IL6R expression increased in Ramos, Daudi, and SU-DHL-10 upon Vincristine treatment, but decreased in OCI-LY3 (Figure 6).

SU-DHL-6 was excluded from the analysis due to consistently high CT values (>35) for all tested genes. Similarly, cells treated with 5 nM Vincristine were excluded for all cell lines except Daudi due to high CT values. Subsequently, each cell line was statistically analyzed by applying a single factor ANOVA to test statistical significance.

In the Daudi cells F was shown to be $> F_{\text{critical}}$. Since $F = 6.13 > F_{\text{critical}} = 3.89$, the difference between groups is statistically significant, which is also underlined by the p-value of 0.0147. The Tukey's HSD test was then applied to identify which groups are different. The test showed no significance for the pairwise comparison of 5 nM Vincr versus 2 nM Vincr (HSD=0.834), and 2 nM Vincr versus Control (HSD=0.446). However, a statistical significance was shown for 5 nM Vincr versus Control (HSD=1.28).

In the Ramos cells the p-value (0.192) is greater than the typical alpha level of 0.05, which means the difference between the treatment and control groups is not statistically significant. The F-statistic (2.031) is less than the F critical value (5.318), also indicating no significant difference.

In the SU-DHL-10 cells the p-value (0.206) is greater than 0.05 meaning the difference between the treatment and control groups is not statistically significant. The F-statistic (2.270) is less than the F critical value (7.709), also indicating no significant difference. While the Vincristine treatment has a much higher average value than the control (5.824 versus 1.000), the large variance in the treatment group (30.755) indicates there was substantial variability in the measurements. This high variability makes it difficult to conclude that the observed difference is due to the treatment. In the OCY-L3 cells the p-value (0.722) is much higher than 0.05, indicating that the difference between treatment and control groups is not statistically significant. The F-statistic (0.139) is substantially lower than the F critical value (5.987), also indicating no significant difference. The high variance in the treatment group (2.727) and the very high p-value suggest that this difference is likely due to random variation rather than a true treatment effect.

These results indicate that high dose Vincristine treatment induces an inflammatory response in the human lymphoma cell Daudi, characterized by the upregulation of IL-6 and variable changes in the expression of CCL5, CXCL10, IL-8, and IL-6R. The inflammatory response and statistical significance varied across different cell lines. However, the consistent upregulation of IL-6 across all cell lines suggests its crucial role in the cellular response to CIN-induction, potentially contributing to drug resistance or other adaptive mechanisms.

IncuCyte Analysis

The study examined the dose-dependent effects of BAY1217389-induced CIN on cell growth and viability in human lymphoma cell lines using Incucyte analysis and Pearson correlation analysis. The research focused on three cell lines: Daudi, Ramos, and SU-DHL-10, each seeded at various densities and treated with BAY1217389 concentrations ranging from 0 to 25 nM over 72 hours.

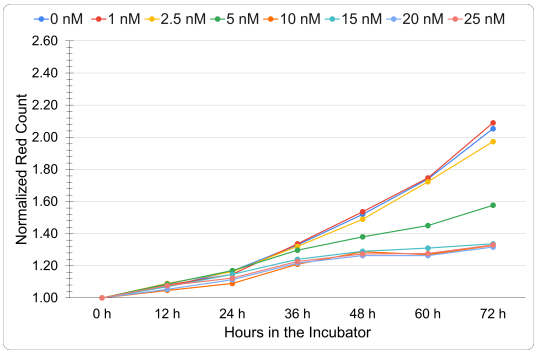

(A)

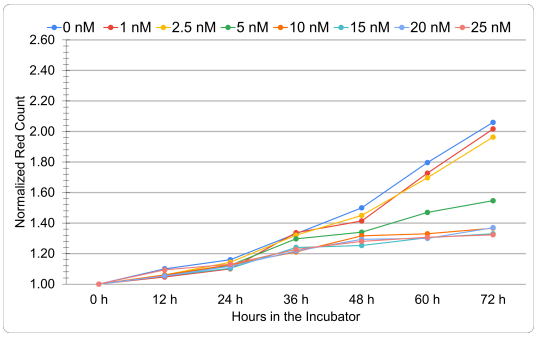

(B)

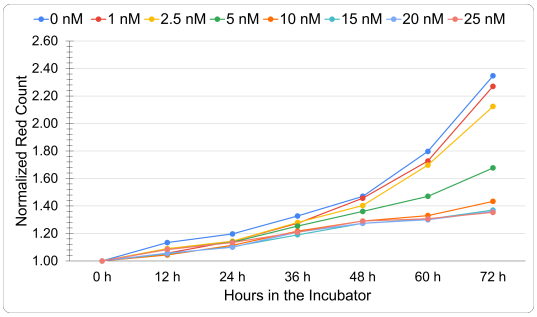

(C)

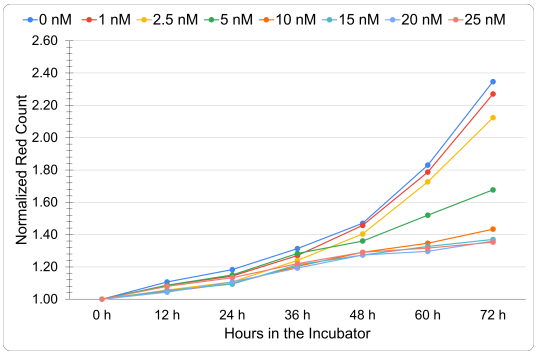

(D)

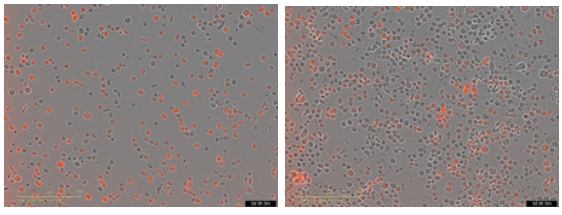

(E) (F)

Figure 7. Growth Rate of Daudi cells treated with 0 nM, 1 nM, 2.5 nM, 5 nM, 10 nM, 15 nM, 20 nM, and 25 nM BAY1217389. (A) Seeding density of 8000 cells. (B) Seeding density of 14000 cells. (C) Seeding density of 20000 cells. (D) Seeding density of 26000 cells. (E) IncuCyte cell image at $t = 0$ hours (left) versus $t = 72$ hours (right).

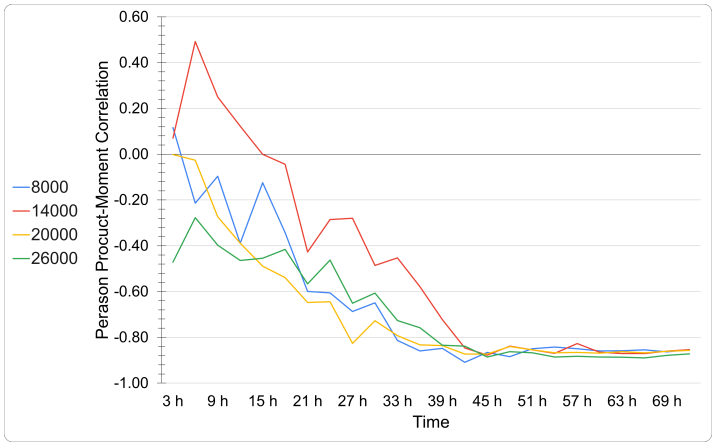

Figure 8. Pearson Product-Moment Correlation between the drug dose and normalized cell count. Quantification of the relationship between BAY1217389 concentration and cell prolifera-tion/viability over time in the Daudi cell line for each seeding density.

In the Daudi cell line higher concentrations of BAY1217389 (≥10 nM) consistently resulted in substantial inhibition of cell proliferation across all seeding densities. The anti-proliferative effects appeared more pronounced at higher cell densities (Figure 7). Pearson correlation analysis revealed strong negative correlations between drug concentration and normalized cell count, emerging rapidly at lower seeding densities and more gradually at higher densities (Figure 8).

The Ramos cell line showed dose-dependent growth inhibition at concentrations ≥5 nM across all seeding densities. Lower seeding densities exhibited more pronounced cytotoxic effects at higher drug concentrations (Figure 9). Pearson correlation analysis demonstrated initially weak correlations that became strongly negative over time, with the highest seeding density showing an initial positive correlation before turning negative (Figure 10).

For SU-DHL-10, concentrations ≥5 nM resulted in dose-dependent growth inhibition across both tested seeding densities. The lower seeding density (8,000 cells/well) showed more potent cytostatic or cytotoxic effects at higher concentrations (Figure 11). Pearson correlation analysis revealed rapid development of strong negative correlations at the lower seeding density, while the higher density initially showed strong positive correlations before shifting to negative values (Figure 12).

Across all cell lines, lower drug concentrations (1 nM and 2.5 nM) did not significantly impair cell proliferation compared to the control, suggesting a threshold concentration for anti-proliferative effects. The varying patterns of response across seeding densities indicate that initial cell density and potential cell-cell interactions may modulate the sensitivity and kinetics of the response to CIN induction.

These findings highlight the complex relationship between CIN induction, cell density, and proliferation in lymphoma cell lines, suggesting that the cellular response to CIN is influenced by both drug concentration and the initial cellular environment.

Discussion

This research aimed to investigate whether CIN in human lymphoma cells activates the IL6-mediated inflammatory signaling pathway and influences their viability, contributing to a pro-tumor microenvironment and modulating therapeutic outcomes. The findings from the genomics analysis, qPCR, and IncuCyte experiments collectively shed light on this research

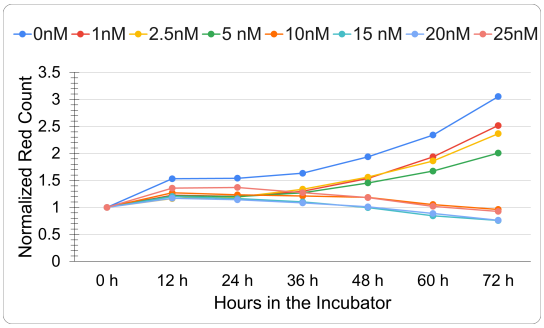

(A)

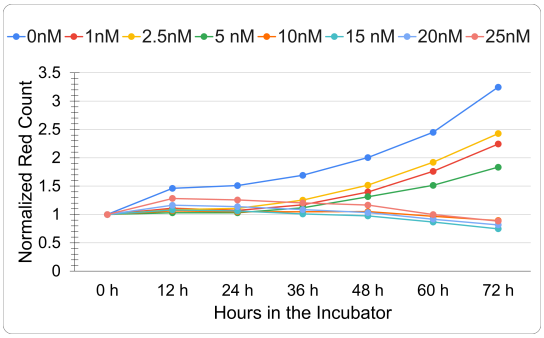

(B)

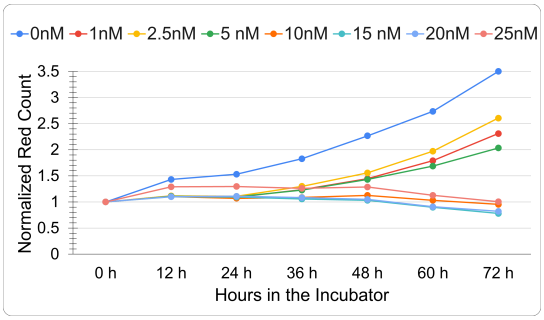

(C)

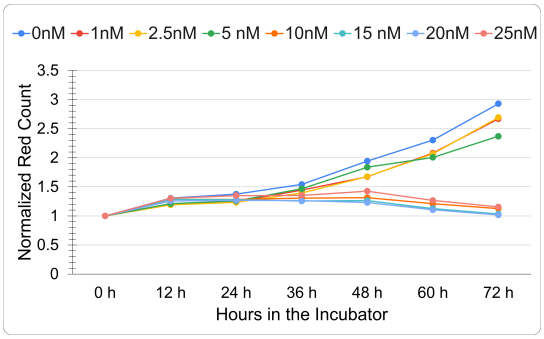

(D)

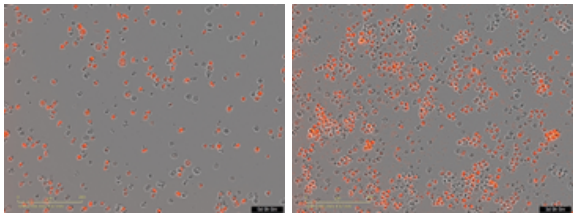

(E) (F)

Figure 9. Growth Rate of Ramos cells treated with 0 nM, 1 nM, 2.5 nM, 5 nM, 10 nM, 15 nM, 20 nM, and 25 nM BAY1217389 (A) Seeding density of 8000 cells. (B) Seeding density of 14000 cells. (C) Seeding density of 20000 cells. (D) Seeding density of 26000 cells. (E) IncuCyte cell image at time point $t = 0$ hours (right) versus $t = 72$ hours (left).

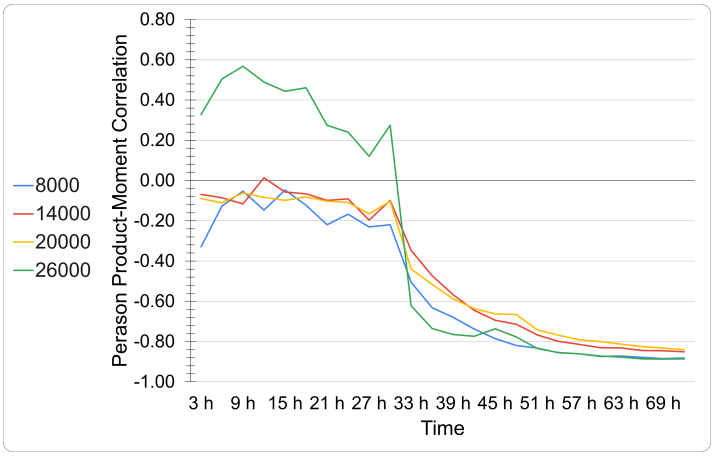

Figure 10. Pearson Product-Moment Correlation between the drug dose and normalized cell count. Quantification of the relationship between BAY1217389 concentration and cell proliferation/viability over time in the Ramos cell line for each seeding density.

question.

Chromosomal Instability

The genomics analysis revealed the diverse mutational landscape and genomic alterations present in the lymphoma cell lines, reflecting their varying degrees of genomic instability. This heterogeneity can promote the survival of subclones with altered inflammatory signaling pathways, as supported by the qPCR results. The OCI-LY3 cell line, with its high degree of genomic instability, demonstrated a substantial 3.78-fold elevation in IL6 expression upon 2 nM Vincristine treatment. This observation suggests that CIN could rewire inflammatory signaling pathways in lymphoma cells to promote tumorigenesis, aligning with findings from Cuceu et al. (2018) and Hong et al. (2022)[1,5].

Role of IL6 in CIN-Mediated Effects

Across all tested cell lines, the qPCR analysis revealed a consistent upregulation of IL6 expression upon Vincristine treatment, corroborating the findings of Hong et al. (2022)[5], who identified IL6 as a key regulator of the inflammatory response in chronic CIN. The SU-DHL-10 cell line, carrying concurrent rearrangements involving oncogenes (MYC and BCL2) and the IGH locus, exhibited the highest change (12.16-fold) in IL6 expression. This observation, coupled with the aggressive clinical course associated with these genetic alterations, suggests the potential role of IL6 in CIN-mediated lymphomagenesis.

While IL6 expression was consistently upregulated, the expression patterns of other cytokines and the IL6 receptor varied across cell lines. This heterogeneity in the inflammatory response, as seen in the qPCR results, could contribute to the differential effects observed in the IncuCyte analysis, where certain doses or cell lines exhibited unique kinetic patterns and responses to CIN induction.

The diverse expression patterns of other cytokines and the IL6 receptor (IL6R) may contribute to the differential effects observed in the IncuCyte analysis, where certain doses or cell lines exhibited unique kinetic patterns and responses to the CIN-inducing agent BAY1217389.

The findings from Hong et al. (2022)[5] provide complementary insights into the role of the IL6R in mediating CIN-induced effects. They observed a positive correlation between IL6R levels and the essentiality of genes involved in DNA repair, chromosome maintenance, and the mitotic spindle

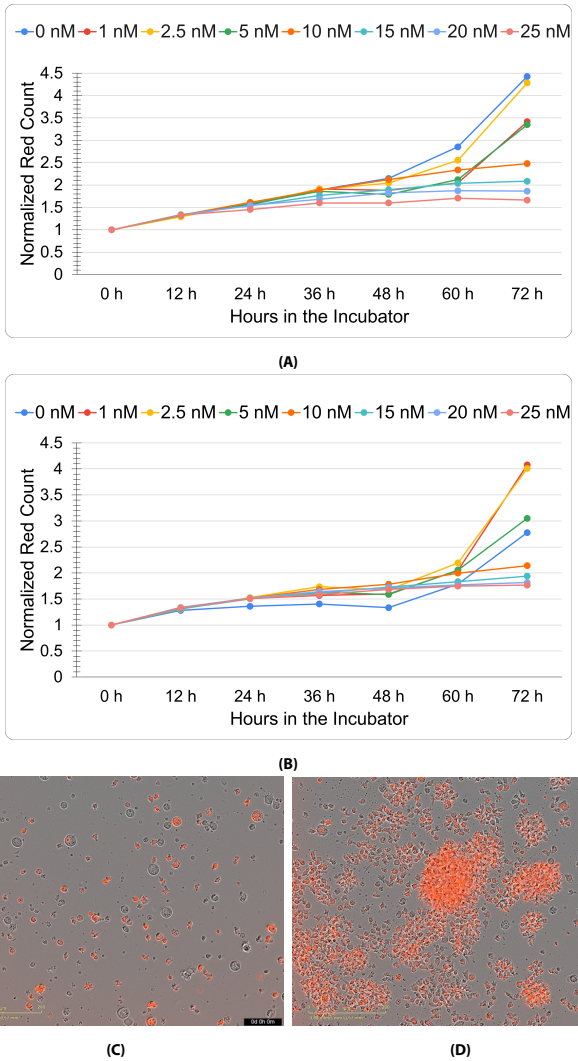

Figure 11. Growth Rate of SU-DHL-10 cells treated with 0 nM, 1 nM, 2.5 nM, 5 nM, 10 nM, 15 nM, 20 nM, and 25 nM BAY1217389. (A) Seeding density of 8000 cells. (B) Seeding density of 14000 cells. (C) IncuCyte cell image at timepoint $t = 72$ hours.

assembly checkpoint. This suggests that cancer cell lines with high IL6R levels are better equipped to regulate CIN across multiple cancer types. In the context of this study, the heterogeneous expression patterns of the IL6R across lymphoma cell lines may contribute to the observed differences in their responses to CIN induction.

Collectively, these findings support the hypothesis that inhibiting IL6 signaling, potentially in combination with CIN-inducing agents like Vincristine or Paclitaxel, could sensitize lymphoma cells to chemotherapy. The differential response to Vincristine treatment among cell lines with varying IL6 and IL6R expression levels further reinforces the notion that modulating the IL6 pathway may enhance therapeutic efficacy in lymphoma patients by targeting the CIN-induced inflammatory signaling mechanisms. However, it should be noted that a statistical significance was not found for all cell lines and all dosages of Vincristine making further research necessary.

Cell Viability After CIN Induction

The IncuCyte analysis revealed a dose-dependent effect of the CIN-inducing agent BAY1217389 on cell viability, with higher doses inducing more pronounced cytotoxic or cytostatic responses across the lymphoma cell lines. Interestingly, certain levels of CIN did not impair, and some

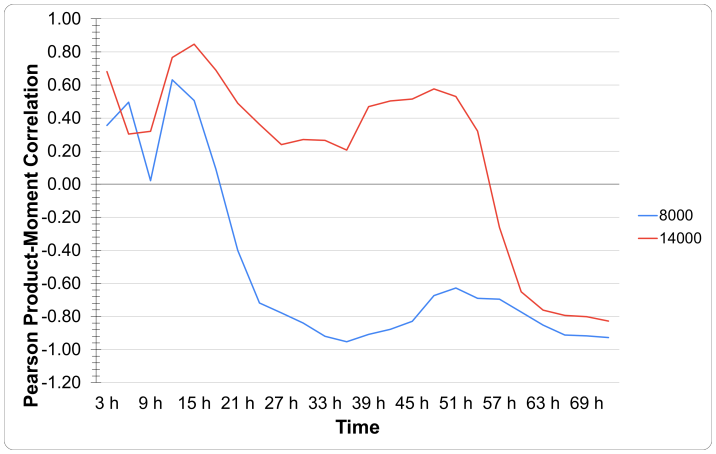

Figure 12. Pearson Product-Moment Correlation between the drug dose and normalized cell count. Quantification of the relationship between BAY1217389 concentration and cell proliferation/viability over time in the SU-DHL-10 cell line for each seeding density.

potentially even enhanced, cell growth in some cell lines, confirming the interplay between CIN and cell survival described by Cuceu et al. (2018)[1]. For instance, in the SU-DHL-10 cell line, lower drug concentrations supported cell growth, while higher concentrations inhibited growth in a dose-dependent manner (Figure 11).

The temporal dynamics and kinetic patterns observed in the IncuCyte analysis varied across doses and cell lines, indicating complex cellular responses to drug exposure and CIN induction. These findings, combined with the heterogeneity in the inflammatory response observed in the qPCR, suggest that CIN not only drives genetic diversity but also influences inflammatory signaling pathways that can modulate drug efficacy and therapeutic outcomes, as proposed by Turner & Reis-Filho (2012) and Hong et al. (2022)[5,14]. Additionally, the degree of cytotoxicity varied across different seeding densities, with lower seeding densities generally exhibiting greater susceptibility to the anti-proliferative and cytotoxic effects of BAY1217389. For instance, in the Ramos cell line, the lowest seeding density of 8,000 c/w showed the most potent cytotoxic effects at higher concentrations (15 nM, 20 nM, and 25 nM) compared to higher seeding densities (Figure 9). This observation suggests that lower cell densities may render lymphoma cells more vulnerable to the anti-proliferative and cytotoxic effects of CIN-inducing agents and that potential cell-cell interactions and cell-heterogeneity may modulate the sensitivity and kinetics of treatment responses.

Implications for Therapeutic Strategies

The consistent upregulation of IL6 expression across cell lines upon Vincristine treatment, as observed in the qPCR, coupled with the dose-dependent effects on cell viability and the differential responses observed in the IncuCyte analysis (Figure 9), support the hypothesis that CIN can activate the IL6-mediated inflammatory signaling pathway in lymphoma cells. The differential response to Vincristine treatment among cell lines with varying IL6 expression levels, as observed in the qPCR, suggests that IL6 may modulate therapeutic response in lymphoma. Combining IL6 inhibitors with standard chemotherapy regimens, such as Vincristine, may enhance therapeutic efficacy in lymphoma patients by targeting the CIN-induced inflammatory signaling pathways.

Limitations and Further Directions

Even though we provided insights into inflammatory signaling in human lymphoma cells, several limitations should be acknowledged. The limited

number of cell lines used in the qPCR analysis and the lack of data for some cytokines due to low cell viability after high-dose Vincristine treatment or double delta Ct values above 35, restricted the generalizability of the findings. The absence of a non-lymphoma cell line as a control group limited the ability to distinguish lymphoma-specific responses from more generalized cellular reactions to CIN-induced stress. The relatively low resolution of the IncuCyte analysis prevented the direct observation of the underlying mechanisms of CIN-induced changes in cell morphology and behavior, limiting the depth of mechanistic insights. As IL6 is a stress cytokine, its upregulation in response to CIN may not be specific to lymphoma cells, and similar responses have been observed in other cell lines, such as breast cancer cells[5]. For the IncuCyte analysis for the SU-DHL-10 cell line, there were not enough cells available after treatment with higher doses of BAY1217389, to test higher seeding densities (20,000 and 26,000 cells), limiting the data analysis. The CIN rates and specific genetic alterations in the cell lines need to be further characterized using techniques like single-cell DNA sequencing to better understand their influence on inflammatory signaling. Future research should focus on addressing these limitations by employing larger sample sizes, including control cell lines, and utilizing higher-resolution techniques to directly observe the effects of CIN on cell behavior and inflammatory signaling.

Conclusion

This research has provided valuable insights into the interplay between CIN, inflammatory signaling, and therapeutic responses in human lymphoma cells. The findings from the genomics analysis, qPCR, and IncuCyte experiments collectively suggested that CIN can activate the IL6-mediated inflammatory signaling pathway in lymphoma cells, contributing to a pro-tumor microenvironment and potentially modulating therapeutic outcomes. The consistent upregulation of IL6 expression observed across multiple lymphoma cell lines upon Vincristine treatment, coupled with the dose-dependent effects of BAY1217389 on cell viability, supports the hypothesis that CIN can influence inflammatory signaling and cellular responses to chemotherapeutic agents. The differential expression patterns of other cytokines and the IL6 receptor across cell lines further underscore the heterogeneity in inflammatory responses, which may contribute to the varying kinetic patterns and therapeutic responses observed in the IncuCyte analysis. By targeting the IL6 signaling axis in combination with standard chemotherapy regimens, it may be possible to enhance therapeutic efficacy and overcome treatment resistance in lymphoma patients. However, further research is necessary to optimize dosing and combinations, as well as to validate the findings in preclinical animal models and clinical studies.

Overall, this research contributes to the growing body of knowledge on the interplay between CIN, inflammatory signaling, and therapeutic responses in cancer, with a specific focus on lymphoma. The insights gained can contribute to the groundwork that might pave the way for the development of innovative therapeutic strategies that leverage the understanding of CIN-induced inflammatory signaling pathways to improve patient outcomes.

Acknowledgments

I would like to express my gratitude to the Laboratory of Genomic Instability in Development and Disease for providing the resources and facilities to conduct my research and experiments for this Paper. I would like to thank my supervisor, Dr. Floris Foijer, for his guidance and support throughout this journey. Moreover, I would also like to extend my thanks to Iris and Merlissa, who supervised me in the Laboratory and gave me valuable insights and explanations. Furthermore, I want to thank the entire team at the Laboratory of Genomic Instability in Development and Disease for creating a collaborative learning environment. Their willingness to answer my questions and share their knowledge was invaluable. Finally, I would like to acknowledge the University College Groningen, especially the science lecturers, for providing me with the foundational knowledge and academic support that laid the groundwork for this research.

References

1. Cuceu, C. et al. Chromosomal instability in Hodgkin lymphoma: an in-depth review and perspectives. *Cancers* **10,** 91 (2018). https://doi.org/10.3390/cancers10040091
2. Siri, S. O., Martino, J. & Gottifredi, V. Structural chromosome instability: types, origins, consequences, and therapeutic opportunities. *Cancers* **13,** 3056 (2021). https://doi.org/10.3390/cancers13123056
3. Kwon, M., Leibowitz, M. L. & Lee, J.-H. Small but mighty: the causes and consequences of micronucleus rupture. *Exp. Mol. Med.* **52,** 1777–1786 (2020). https://doi.org/10.1038/s12276-020-00529-z
4. Afonso, O., Figueiredo, A. C. & Maiato, H. Late mitotic functions of Aurora kinases. *Chromosoma* **126,** 93–103 (2017). https://doi.org/10.1007/s00412-016-0594-5
5. Hong, C. et al. cGAS–STING drives the IL-6-dependent survival of chromosomally instable cancers. *Nature* **607,** 366–373 (2022). https://doi.org/10.1038/s41586-022-04847-2
6. Kadowaki, H. & Nishitoh, H. Signaling pathways from the endoplasmic reticulum and their roles in disease. *Genes* **4,** 306–333 (2013). https://doi.org/10.3390/genes4030306
7. Chen, X., Shi, C., He, M., Xiong, S. & Xia, X. Endoplasmic reticulum stress: molecular mechanism and therapeutic targets. *Signal Transduct. Target. Ther.* **8,** 352 (2023). https://doi.org/10.1038/s41392-023-01570-w
8. Kwon, J. & Bakhoum, S. F. The cytosolic DNA-sensing cGAS–STING pathway in cancer. *Cancer Discov.* **10,** 26–39 (2020). https://doi.org/10.1158/2159-8290.CD-19-0761
9. Shi, Z. et al. Activation of the PERK-ATF4 pathway promotes chemo-resistance in colon cancer cells. *Sci. Rep.* **9,** 3210 (2019). https://doi.org/10.1038/s41598-019-39547-x
10. Wegiel, B., Bjartell, A., Culig, Z. & Persson, J. L. Interleukin-6 activates PI3K/Akt pathway and regulates cyclin A1 to promote prostate cancer cell survival. *Int. J. Cancer* **122,** 1521–1529 (2008). https://doi.org/10.1002/ijc.23261
11. Sempere, M. C., Fanjul, V. R., Pérez, I. S. & Perona, R. The role of the NFκB signalling pathway in cancer. *Clin. Transl. Oncol.* **10,** 143–147 (2008). https://doi.org/10.1007/s12094-008-0171-3
12. Johnson, D. E., O'Keefe, R. A. & Grandis, J. R. Targeting the IL-6/JAK/STAT3 signalling axis in cancer. *Nat. Rev. Clin. Oncol.* **15,** 234–248 (2018). https://doi.org/10.1038/nrclinonc.2018.8
13. Braicu, C. et al. A comprehensive review on MAPK: a promising therapeutic target in cancer. *Cancers* **11,** 1618 (2019). https://doi.org/10.3390/cancers11101618
14. Turner, N. C. & Reis-Filho, J. S. Genetic heterogeneity and cancer drug resistance. *Lancet Oncol.* **13,** e178–e185 (2012). https://doi.org/10.1016/s1470-2045(11)70335-7